

# Physics-based broadband ground-motion simulations: rupture dynamics combined with seismic scattering in a heterogeneous Earth crust

**P. M. Mai**

*Division of Physical Sciences and Engineering KAUST, Thuwal, 23955-6900, Saudi Arabia*

**L. A. Dalguer**

*Swiss Seismological Service (SED-ETHZ), Zürich, Switzerland*



## SUMMARY:

Simulating realistic broadband ground-motions for earthquake engineering applications is a key challenge in earthquake seismology. We present a novel approach to compute fully physics-based near-field synthetic seismograms in a wide frequency band. In our work, we combine spontaneous dynamic rupture modeling with a high-frequency seismic-scattering approach to generate broadband (0 - 20 Hz) near-source seismograms. Our modeling considers buried and surface-rupturing faults on which strike-slip, normal-faulting, and reverse-motion scenario earthquakes occur, embedded in a layered velocity-density model with constant or depth-dependent normal stress. Each scenario event is modeled with an initial random stress field that then generates a physically self-consistent complex rupture evolution, including heterogeneous slip, variable rise time (slip-rate function), and complicated rupture propagation. From the spontaneous dynamic rupture calculations we obtain the low-frequency (LF:  $f < 3\text{Hz}$ ) seismic wave field. We then combine the LF-seismograms with a high-frequency (HF:  $f > 2\text{Hz}$ ) scattered seismic wavefield, computed using multiple backward-S-to-S scattering. The scattering parameters are chosen based on regional studies on seismic coda, and calibrated against ground-motion prediction equations. Hybrid broadband waveforms are obtained by combining the high-frequency scattering seismograms with the low-frequency rupture-dynamics wavefield using a simultaneous amplitude-phase matching algorithm. We apply our method a large number of dynamic rupture models for  $\sim M 6.5$  thrust-faulting, normal-faulting and strike-slip earthquakes, either buried or allowed to break the surface, under depth-dependent and constant normal stress on the fault. The set of scenario earthquakes generates a wide range of ground-shaking behavior. Comparing against modern ground-motion prediction equations, within a given faulting style and magnitude range, we find (i) larger ground-motion variability but comparable median values; (ii) cases for extreme ground-motions; (iii) surprising reduction in shaking levels in the very near-field of the rupture ( $R < 5\text{ km}$ ). These results are stable with respect to different choices of realistic scattering parameters. Examining the prediction bias for ensembles of scenario events, we suggest that our approach may provide a methodology for simulation-based seismic hazard assessment. Our results also imply that ground-motion uncertainty in the very near-field ( $R < 5\text{ km}$ ) of moderate-to-large earthquakes may be higher than at larger distances

*Keywords: near-field broad-band ground motion simulations, rupture dynamics, seismic scattering*

## 1. INTRODUCTION

Broadband (0 – 20Hz) ground-motion simulation for earthquake-engineering and seismic-hazard purposes is a key research topic in earthquake seismology. However, it is also one of the most challenging problems, as one needs to simultaneously consider the complexity of the earthquake rupture process, the intricacies of seismic wave-propagation through heterogeneous Earth structure and shaking (de-)amplifications due to local site effects. Each of these physical phenomena represents its own research field; creating “end-to-end” simulations that include all three of the fields for realistic ground-motion prediction is thus a difficult task. In this context, we discriminate between ground-

motion simulations and ground-motion prediction. While the former attempt to create realistic time series of ground-shaking at selected sites over a generally limited frequency range, the latter employ empirical ground-motion prediction equations (GMPE's) to calculate a few indicative ground-motion parameters (peak-ground acceleration, PGA; peak-ground velocity, PGV; spectral acceleration at selected periods  $T$ ,  $SA_T$ ). While simulation approaches suffer from limiting assumptions in the modeling setup (for the rupture process and Earth structure) and are computationally expensive, they have the advantage of being in principle more realistic; they also provide full time histories needed in nonlinear structural analysis. In contrast, GMPE's are simple to apply, but insufficient for nonlinear structural analysis. For adequate prediction of near-source ground motion and seismic hazard analysis, GMPE's suffer from hard-to-quantify variability and not-well-understood saturation effects at close distance. These deficiencies arise because GMPE's are derived from sparse recorded data, and hence cannot capture effects of complex rupture processes, wave-propagation in heterogeneous Earth, and local site amplification. Accurate physics-based numerical modeling with realistic earthquake source complexity and wave-propagation in 3D Earth is needed to completely capture the level and variability of near-source ground motions.

Many recent damaging crustal earthquakes exhibited very large ground-accelerations that frequently exceed  $1g$  ( $M_w$  6.9 2008 Iwate-Miyagi Nairiku earthquake (Japan);  $M_w$  7.0 2010 Darfield event (NZL);  $M_w$  6.3 2011 Christchurch earthquake (NZL)). Besides very large shaking levels in the frequency range of engineering interest (up to 10 Hz), large motions were also observed at relatively low frequencies  $\sim 1.0$ Hz (e.g. in the 2011  $M_w$  6.3 Christchurch earthquake). An additional observation is that the spatial ground-motion variability is very high (e.g. for the  $M_w$  6.0 2004 Parkfield earthquake where shaking levels over  $1g$  were observed very close to other sites that only showed moderate shaking levels; Shakal et al, 2006). As summarized by Mai (2009), the variability of recent ground-motion observations often exceeds the ground-motion variability predicted by current GMPE's. Additionally, the saturation effects at very close distances have been questioned (where GMPE's predict constant shaking levels for distances less than  $\sim 5$  km from the fault) using advanced numerical simulation results (e.g. Guatteri et al, 2003; Ripperger et al, 2008) and recent observations that indicate that very near-field shaking may in fact decrease (on average) compared to current GMPE's.

The above introduction illustrates the need for advanced broadband ground-motion simulations that account for complexity in the source, scattering in seismic wave propagation, and local site-amplification effects, to better explain and reproduce recent observations on the level and variability of near-field ground motions. The present study comprises dynamic rupture modeling and hybrid broadband ground-motion calculations, focusing on combining low-frequency ( $f < 3$  Hz) seismograms that contain the signature of realistically complicated source with high-frequency seismograms that capture scattering effects along the path from the source to the bedrock site. We do not consider local site effects (site amplification or nonlinear site response) in the present study.

## 2. METHODS

### 2.1 Dynamic rupture modeling

The details of our dynamic rupture calculations are given in Dalguer and Mai (2011), and are only briefly summarized. We assume a fractal initial stress distribution on the rupture plane that is embedded in a one-dimensional velocity-density structure. One suite of simulations assumes constant normal stress, an alternative set utilizes depth-dependent normal stress. We adopt a linear slip-weakening model with constant slip-weakening distance in the center of the fault, increasing to larger

values in a 3-km wide buffer zone at the fault boundaries to ensure smooth rupture stopping. We consider ruptures that remain buried (top edge of rupture at 5km depth), and events that are allowed to break the surface. Because the potential faulting-style for these scenario events is not known a priori, we consider a vertical strike-slip rupture plane, a 60°-dipping normal fault, and a 45°-dipping reverse fault. Since we generate 30 realizations of initial stress (parameterized in terms of von Karman correlation function) for each case, we simulate a total of 360 spontaneous dynamic ruptures. The target (maximum) source dimensions follow source-scaling relations (e.g. Mai & Beroza, 2000). The complete dynamic rupture calculations thus provide fully physics-based finite-fault rupture models with spatial heterogeneity in the kinematic source parameters slip, slip-velocity, and rupture time; from the dynamic rupture simulations we then extract low-frequency ( $f_{\max} \sim 3$  Hz) seismograms at a dense station array.

## 2.2 Broadband ground-motion simulations

To generate broadband time series for engineering purposes, into the frequency range up to  $\sim 50$  Hz, several methods have been devised in the recent past in which an “arbitrary” stochastic high-frequency (HF) signal is added to pre-computed low-frequency (LF) wavefield. This addition is carried out either in the time-domain (Berge et al, 1998) or in the frequency domain (Graves and Pitarka, 2004) at some pre-selected and fixed matching frequency. However, in these calculations, the phase-angles of the waveforms are not considered. Owing also to a spectral-amplitude mismatch between the LF and HF signal at the fixed matching frequency, the resulting broadband signal are often found to be “energy-deficient” around the matching frequency (Cornell, pers. communication, 2000). What that essentially means is that the building response at corresponding periods, computed from such simulated broadband seismograms, is often inconsistent with the one computed from actual data.

Mai and Beroza (2003) proposed a hybrid approach for broadband ground-motion computations in which the matching frequency for the LF and HF signal is found through an optimization that minimizes the amplitude and phase mismatch between the two signals. The optimization operates in a narrow frequency range (0.1 – 0.2 Hz) around a target matching frequency; the matching thus depends on the individual LF- and HF-time series, and may be different for each component of motion.

For computing the HF-frequency wavefield, we refrain from using “standard” engineering tools to generate stochastic point-source accelerograms (e.g. Boore, 1983). Instead, we compute elementary scattering “Greens functions” utilizing the multiple-scattering theory of Zeng (1991) and Zeng et al. (1993). These scattering wavelets are then convolved with a moment-rate function representing the temporal rupture evolution; following the work of Mena et al. (2010), we use the source-time function described by Dreger et al. (2007). These site-specific scattering operators are then used to form the HF-signal for each station (Mai et al, 2010). Performing the frequency-domain combination of the HF- and LF-signals finally provides simulated broadband seismic signal that are characterized by self-consistent physics both in the rupture process (dominating the long-period motions) and wave-propagation in heterogeneous media (high-frequency scattering).

In this study, we use scattering parameters following Edwards et al. (2009).  $Q_0$  is assumed to represent the average crustal attenuation (Anderson and Hough 1984); based on Edwards et al. (2009) we choose  $Q_0 = 1300$ . We select the corresponding site-kappa as  $\kappa = 0.01$ , in agreement with the site-specific kappa-values inferred at the site of interest (Edwards et al., 2009). The elastic-wave scattering parameter  $\eta_s$  is selected to be 0.03, representing a mean-free path-length of  $\sim 30$  km. However, the final ground-motion results are not very sensitive to the particular choice of  $\eta_s$ , as reported by Mena et

al. (2010). Additionally, we apply a generic site-amplification function (Borcherdt 1994, 2002) to account for the fact that the dynamic simulations consider a minimum shear-wave speed of 2500 m/s, which is not representative for strong-motion recordings and ground-motion prediction equations derived from strong-motion data. We apply site-amplification function for a minimum shear-wave speed of 1500 m/s. From our dynamically consistent broadband ground-motion simulations we then obtain synthetic seismograms for which ground-motion parameters of interest (PGA, PGV, SA at various periods T) are compared against several recent ground-motion prediction equations.

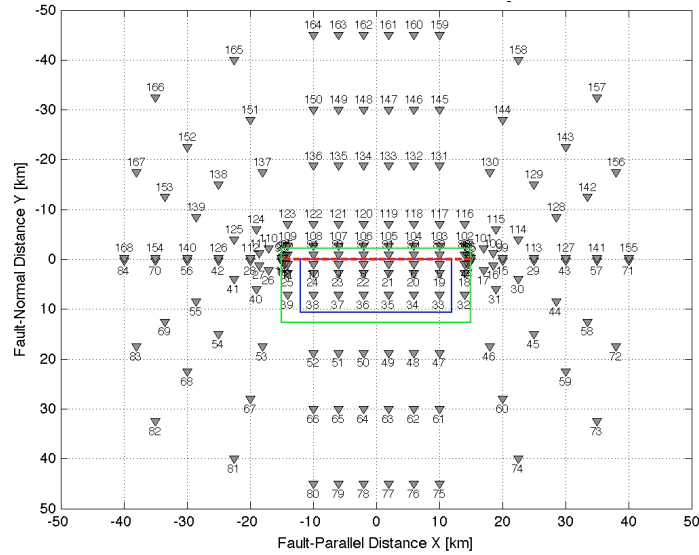


**Figure 2.1.** Station and fault geometry for broadband ground-motion simulations. The thick red-line marks the vertical projection of the top-edge of the targeted rupture plane (in blue), the green dotted lines mark the vertical projection of maximum allowed fault plane.

We compute ground-motions on a virtual receiver array that is arranged around the fault (Figure 2.1). For dipping faults there are 168 stations, for the strike-slip case correspondingly 84 stations, in a distance range  $0 \leq R_{JB} \leq 80$  km. Several stations are close to being nodal for the S-wave radiation pattern for the strike-slip earthquakes. For the sites with fault-normal position Y being 1 km or less, the wave-amplitudes on the fault-parallel-component of motion is very small, while all the seismically radiated energy is concentrated on fault-normal-component of motion and the vertical component.

Broadband ground-motions synthetics are generated with 48sec duration, with a nominal maximum frequency of the seismograms of 100 Hz, while the reliable frequency range extends only to  $\sim 50$  Hz. As seen in then waveform examples in Figure 3.1 and 3.2, the amplitude-spectral decay falls off more rapidly than the expected  $1/f$  (in velocity) beyond  $f_{max} \sim 50$  Hz due to numerical inaccuracies at the highest frequencies.

### 2.3 Site kappa, scattering parameters, and broadband waveform generation

The spectral decay of the recorded seismic waves at high frequencies can be described by the expression  $A(f) = A_0 \exp [-\pi \kappa f]$ , where  $A_0$  is the reference amplitude,  $f$  is frequency, and the spectral decay parameters  $\kappa$  is site-kappa. Generally,  $\kappa$  is smaller on rock sites, and higher on alluvium sites, i.e. low  $\kappa$  mean more efficient propagation of high-frequency seismic energy. In our study, we test several site-kappa values in the vicinity of the results of Edwards et al. (2009) who performed a

detailed kappa-study close to the site of interest. Their  $\kappa$ -values fall in the general range  $\kappa = 0.02 \pm 0.005$ . We test  $\kappa = 0.01$  and  $\kappa = 0.03$  in our broadband computations; since the overall results do not change drastically, we report our findings for  $\kappa = 0.01$  only.

To test the sensitivity of the broadband motions to variations in the scattering parameters, we perform multiple broadband-computations for a subset of scenarios. These tests are not meant to define an “optimal” parameter set, but rather to assess the variability of ground-motion amplitudes for changes in the scattering parameters. In particular we test:

- The elastic scattering coefficient,  $\eta_s$ , in the range  $0.01 \leq \eta_s \leq 0.05$
- The average-crustal attenuation,  $Q_0$ , in the range  $100 \leq Q_0 \leq 0.05$
- The frequency-decay parameter,  $\alpha$ , in the range  $0.5 \leq \alpha \leq 1.0$
- The target matching frequency,  $f_m$ , in the range  $0.2 \leq f_m \leq 1.0$

Considering variations in the elastic scattering coefficient,  $\eta_s$ , ground-motion amplitudes for PGA and spectral acceleration at short periods vary by at most  $\pm 10\%$ , but generally remain within  $\pm 5\%$  from the values for  $\eta_s \leq 0.03$  (consistent with findings of Mena et al, 2010). A similar variation is achieved simply by using different random-number seeds for generating the stochastic wavelets. The attenuation  $Q_0$ , representing the average crustal attenuation, is changed according to the findings by Edwards et al. (2009) and within a range of  $Q$ -values given in the literature. For  $Q_0$  lower than about 300, the amplitude-versus-distance decrease of ground-motions is too rapid, leading to strong under-predictions at larger distances. We thus do not further consider  $Q_0 < 300$ . Values of  $Q_0 \geq 500$  provide reasonable amplitude-distance decay; increasing  $Q_0$  above 700 result in ground-motion amplitudes consistent with ground-motion prediction equations (e.g. Akkar & Bommer, 2010), while further increasing  $Q_0$  to 1300 (Edwards et al, 2009) amplifies the high-frequency motions only by 2-3 %. For internal consistency we select  $Q_0 = 1300$  for our final set of simulations.

The implementation of the multiple-scattering theory (Zeng et al., 1991; Zeng, 1993) only considers the wave-amplitude attenuation due to elastic wave-scattering in a heterogeneous medium. To account for anelastic (intrinsic) attenuation, the common model of a frequency-dependent path-attenuation  $Q(f) = Q_0 f^\alpha$  is used (e.g. Anderson and Hough, 1984; Atkinson and Silva, 1997), with the frequency-decay parameter  $\alpha$ . In the corresponding literature a range of  $\alpha$ -values is discussed, where  $0 \leq \alpha \leq 1$ , and the value of being regional dependent. Common values for the decay parameter are  $0.5 \leq \alpha \leq 0.8$ . We test a range of values, but did not find very strong effect on ground-motion amplitude, aside from slide amplitude decrease for lower values of  $\alpha$ . We thus use  $\alpha = 0.7$  in our simulations, consistent with Atkinson and Silva (1997) and Mena et al. (2010).

Our broadband approach requires a target matching frequency. In most schemes for hybrid broadband computations (e.g. Graves and Pitarka, 2010), this transition frequency is fixed (e.g. to  $f_m = 1\text{Hz}$ ) with the notion that wave-propagation in heterogeneous Earth is to a large extent deterministic at frequencies below 1 Hz, and tends to be increasingly stochastic at frequencies above 1Hz. Several studies report the loss (or at least a strong decrease) of directivity effects at frequencies above 1 Hz (e.g. Spudich and Chiou, 2008; Pulido and Kudo, 2004). In our simulation we assume a planar fault and a one-dimensional velocity-density profile, resulting in strong directivity effects due to the relative smoothness and coherence of the rupture evolution and the simplified wave-propagation. In nature, complex faulting geometry as well as heterogeneous Earth structure contribute to the breakdown of rupture coherency, which decreases directivity effects and increases high-frequency radiation.

Therefore, we base the matching frequency on an estimate of the corner frequency of each individual rupture model in our set of 360 simulated events. For smaller earthquakes with higher corner frequency the matching frequency will be higher, reflecting the generally higher frequency content of smaller earthquakes. The approximate corner frequency  $f_c$  is computed using the circular-rupture, constant stress-drop, fixed rupture-speed model,  $f_c = 0.42 \cdot \beta \cdot (\Delta\sigma/M_0)^{1/3}$  where  $\beta$  is the shear-wave speed at the source (in our case hypocenter) and  $\Delta\sigma$  is the average stress-drop over the effective rupture area. A number of tests reveal that  $f_m = 3 f_c$  as matching frequency provides consistent results with respect to the GMPEs; we find a minimum  $f_m \sim 1.0$  Hz for the smallest events in our database of simulated events ( $M_w \sim 5.7$ ) and a maximum  $f_m \sim 0.2$  Hz for the largest scenario ruptures (an  $M_w \sim 7.1$ ).

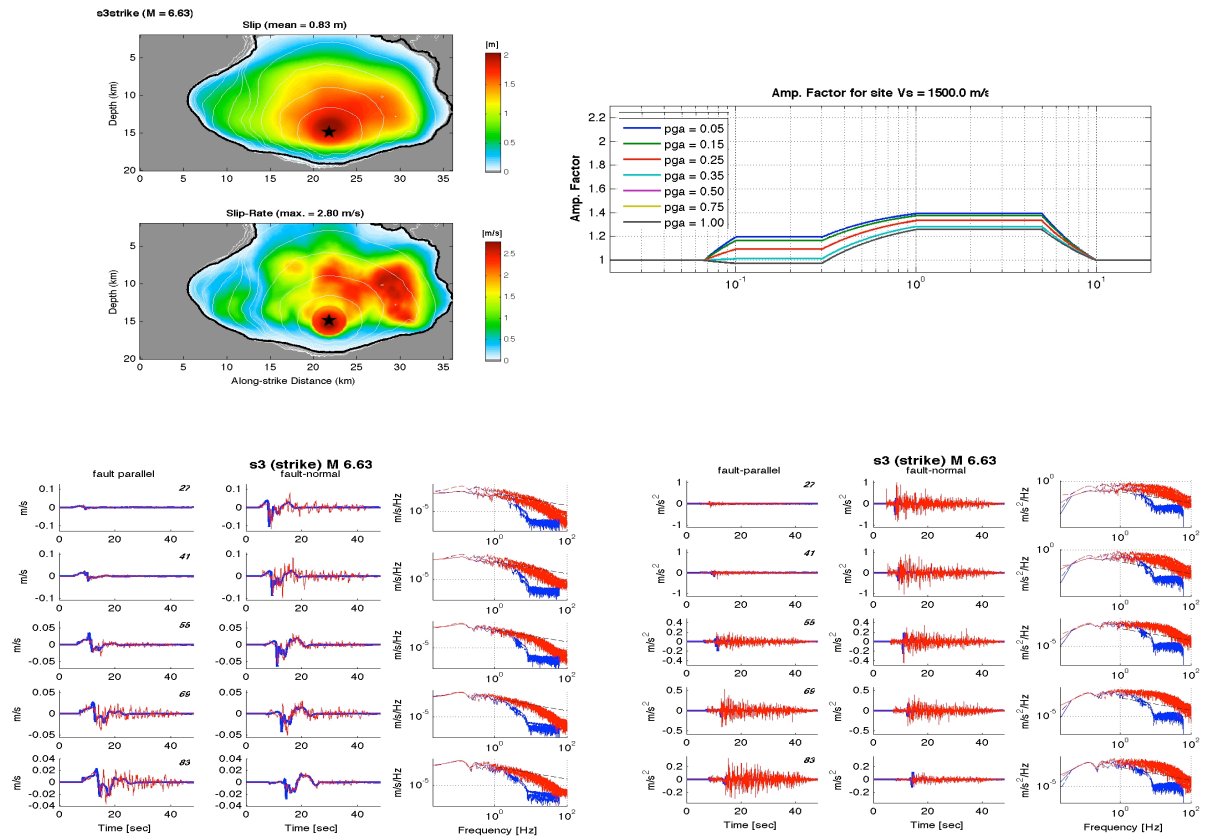
### 3. BROADBAND GROUND MOTION: WAVEFORMS & COMPARISON WITH GMPE

Ground-motion parameters computed from the broadband time histories are PGA, PGV, and spectral acceleration ( $SA_T$ ) at a range of periods,  $T$ . Response spectral values were computed with the Newmark-method for linear systems for the two horizontal components of motion (fault-normal Y, and fault-parallel X). For each GMP, we report the value of the geometric mean of the two horizontal components, computed as  $GMP = \sqrt{GMP_x \cdot GMP_y}$ . For each scenario event we apply site-amplification corrections to properly scale synthetics from the minimum shear-wave speed of 2500 m/s used in the dynamic calculations to a more typical  $V_{s30}$ -values of 1500 m/s. The site-amplification corrections use period-dependent amplification coefficient of Borchardt (1994; 2002), applied to the Fourier-amplitude spectrum of the simulated waveforms. We adopt  $V_{s30} = 1500$  m/s for site-correction instead of a more common value of 760 m/s (or even lower) since the applicability of the Borchardt-approach to such strong alterations is not well tested. However, scaling to such low  $V_{s30}$  would provide an additional amplitude increase of about a factor 1.2 – 1.5. Figure 3.1 provides an example of our hybrid broadband approach for one dynamic rupture and displays resulting waveforms and Fourier amplitude spectra (in velocity and acceleration) at several near-fault sites.

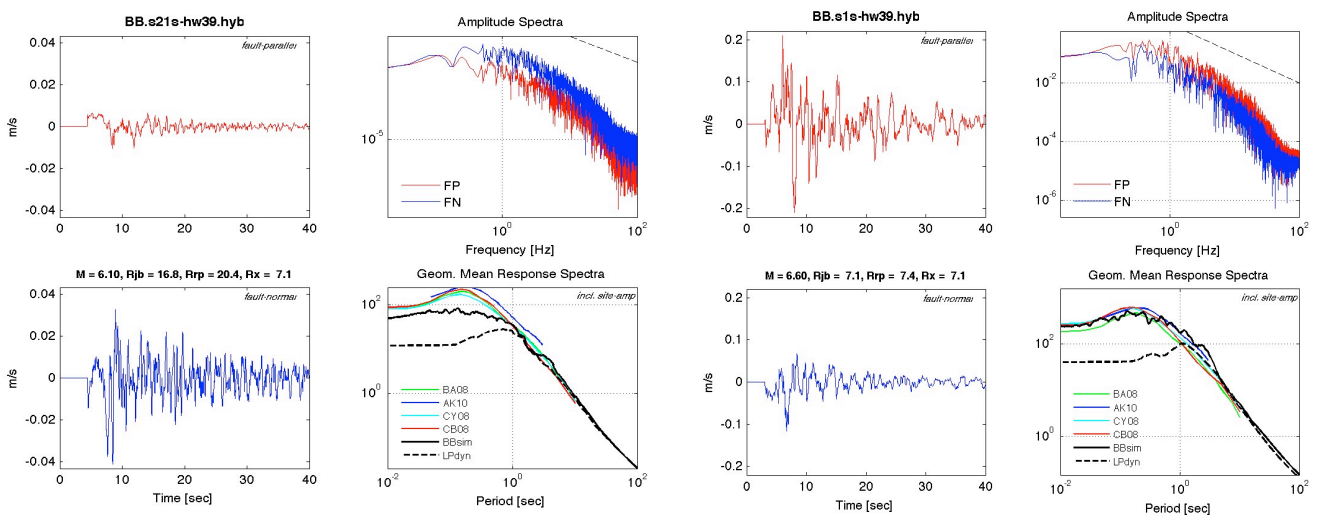
We do not aim to deliver a set of waveforms for immediate engineering use; rather we examine to what extent the current dynamically constrained broadband simulations are consistent with empirical predictions. If the simulations are in agreement with the empirical predictions, but show deviations from GMPE's or specific characteristics in the distance range of sparse observations (i.e. in the very near-source region), then future near-source ground-motion may be more adequately estimated using simulations rather than empirical predictions. For the following discussion it is important to note that we have made no attempt to optimize our parameterizations to match any empirical equation. All simulations are done with the same scattering-parameter set and site-amplification factors

Figure 3.2 displays two representative examples of broadband time series, their amplitude spectra, and the resulting geometric mean of spectral acceleration. As can be seen, the broadband time series exhibit a strong signature of the high-frequency scattering, which is evident also in the amplitude spectra that decay as  $1/\text{frequency}$  above the matching frequency ( $f_m \sim 0.2\text{-}3$  Hz in Figure 3), and out to  $\sim 50$  Hz. However, the response-spectral characteristics, here compared in terms of the geometric mean, do not necessarily match the empirical predictions, despite the amplitude spectra appear to be “complete” in their frequency content.

In Figure 3.3, we compare selected parameters for a set of scenarios, showing ground-motion parameters for a buried  $M_w$  6.62 strike-slip scenario compared to empirical predictions by Boore & Atkinson (2008) and Akkar & Bommer (2010), and ground-motions resulting from the same hetero-



**Figure 3.1.** (Top-left) Example dynamic rupture model (buried M 6.33 strike-slip), with colored slip and slip-velocity and white rupture-time contours; (Top-right) Site-amplification factors (Borcherdt, 1994; 2002) for different input PGA (colored lines) to scale ground-motions from input site  $V_{S30}$  of 2500 m/s to  $V_{S30} = 1500$  m/s (Bottom) Example hybrid broadband waveforms for above rupture model at five stations with increasing distance from the fault (left: velocity; right: acceleration). Broadband time series and amplitude spectra (right-most column) are plotted in red, low-frequency synthetics from dynamic calculations are shown in blue.



**Figure 3.2.** (Left frames) Fault-parallel (top-left) and fault-normal (bottom-left) ground-motion for an  $M_w$  6.1 strike-slip rupture at  $\sim 16$  km distance. The velocity-amplitude spectra (top-right) display an approximate  $1/f$  decay up to  $\sim 50$  Hz. The broadband spectral response roughly matches empirical prediction (bottom-right), while the LF-response spectra cannot match the short periods. (Right frames) Same as left frames, but for an  $M_w$  6.6 event at  $\sim 7$  km distance. In this case, the resulting spectral response matches the empirical predictions.

-ogeneous stress field, but allowed to break the free surface. The resulting event has increased magnitude,  $M_w$  6.75, and hence also stronger shaking. In both cases, the simulations exhibit the same distance-decay as the empirical curves. Shaking levels generally agree with GMPE's predictions, but indicate higher-than-empirically-predicted variability. A similar pattern can be seen if the same initial stress is resolved on  $45^\circ$ -dipping faults to generate surface-breaking reverse-faulting earthquake.

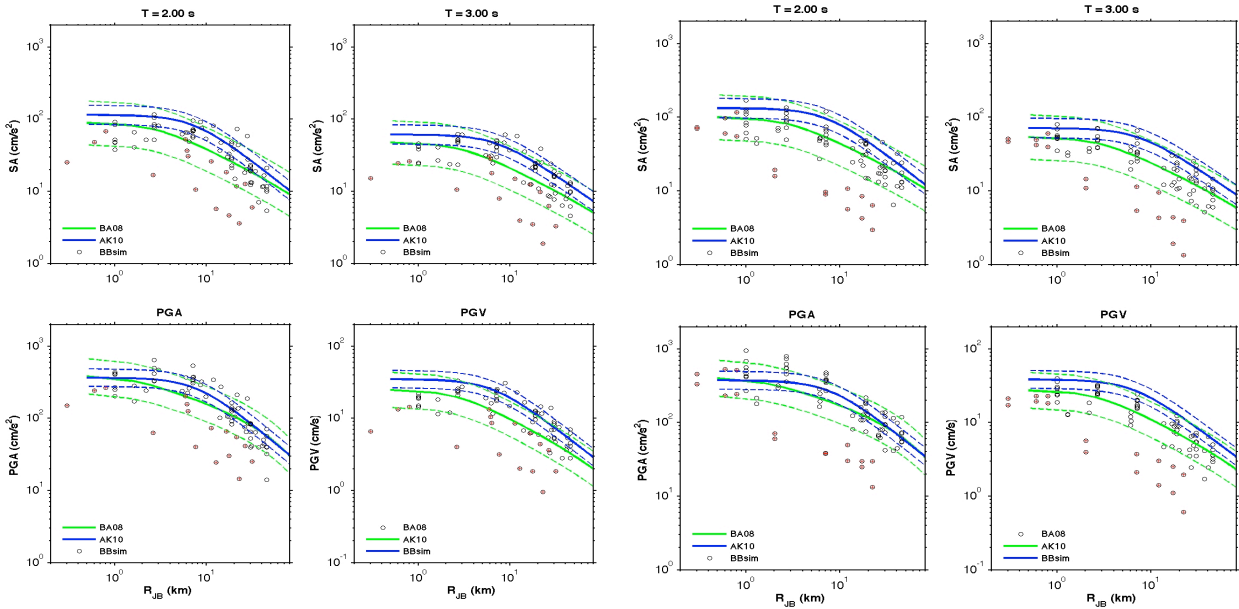


**Figure 3.3:** Ground-motion parameters for buried  $M_w$  6.62 strike-slip earthquake (left four frames) and a surface-breaking  $M$  6.75 strike-slip event (right four frames), both with the same initial stress field. Comparisons are made to the GMPE's by Akkar and Bommer (2010; blue) and Boore and Atkinson (2008; green). Dotted lines mark  $\pm 1\sigma$  bounds. Simulation-data marked with a red-cross are close-to nodal for strike-slip ruptures.

We find that for a given random initial dynamic stress, the surface-breaking earthquakes have higher magnitude than the buried events, due to increased slip in the shallow parts of the fault. Magnitudes for the strike-slip and normal events are comparable, but magnitudes of thrust-faulting events are consistently 0.2-0.3 higher. Adding to the magnitude difference the general pattern of larger ground-motions for reverse-faulting events (compared to strike-slip and normal faulting earthquakes) for the same magnitude, we find that – for identical initial random stress on the fault – the thrust-faulting ruptures have considerably higher shaking levels than the strike-slip and normal-faulting ruptures.

Figure 3.4 plots ground-motions obtained from multiple events within a given magnitude bin, grouping ruptures within  $M \pm \Delta M$ , where  $\Delta M = 0.1$ . Comparisons are made with respect to GMPE's for the center magnitude  $M$ , hence considerable under- and over-predictions are expected. Figure 3.4 shows that the overall ground-motion level for the buried and surface-rupturing events agrees with the empirical predictions. For strike-slip events, many close-to-nodal sites display expected low shaking (marked by red crosses). Additionally, we find an indication for reduced motions (compared to GMPE's) at very close distances ( $R_{JB} < 3$  km), which is most pronounced for buried strike-slip scenarios. While the distance decay of our simulations is consistent with the GMPE's, we find that the ground-motion variability in our results appears to exceed the uncertainties given in the GMPE's.

Examining the resulting variability  $\sigma_{\ln Y}$  of the hybrid broadband ground-motions, we notice that  $\sigma_{\ln Y}$  is generally close to  $\sigma_{\ln Y} = 0.5$ , oscillating between  $\sigma_{\ln Y} = 0.4$  to  $\sigma_{\ln Y} = 0.7$ , with only mild dependency of  $\sigma_{\ln Y}$  on the distance. Normal-faulting and strike-slip ruptures exhibit a very similar behavior, while the variability for reverse-faulting events appears to be slightly lower. We do not find evidence for any magnitude dependence of ground-motion variability. Interestingly, we observe a small increase in  $\sigma_{\ln Y}$ -values for surface-rupturing events, associated to the location of sites with respect to where the surface rupture occurs. For buried events, even close-in sites are located a considerable distance away from large on-fault slip regions. Thus, we hypothesize that sites of extreme motions are located close to surface-breaking areas or in regions of enhanced on-fault directivity (Mena and Mai, 2011).

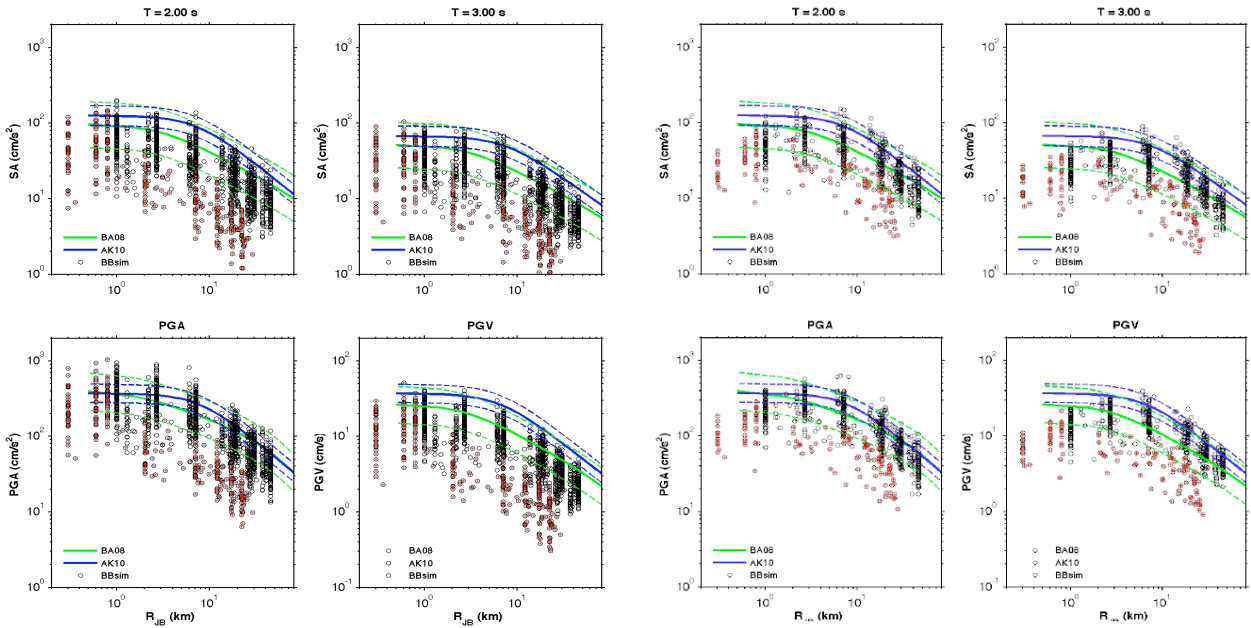


**Figure 3.4:** Similar to Figure 3.3 a 19 surface rupturing strike-slip earthquakes ( $6.6 \leq M_w < 6.8$ ; left four frames) and 8 buried strike-slip events ( $6.6 \leq M_w < 6.8$ ; right four frames).

#### 4. CONCLUSIONS

Using spontaneous dynamic rupture simulations for strike-slip, normal-faulting, and thrust-faulting earthquakes, we compute hybrid broadband ground-motions. Long-period seismic waveforms are combined with high-frequency scattering Green's function to form physics-based broadband near-field seismograms. The resulting three-component seismograms are then compared with ground-motion prediction equations. Our findings indicate that dynamically constrained broadband motions generally agree with empirical predictions, as they capture correctly the overall characteristics of the predicted motions. Deviations exist in the near-field, where the simulation display larger variability as well an overall decrease of the shaking levels at very close distances for strike-slip rupture. Additional discrepancies between simulations and GMPE's are due to incomplete accounting for local site amplification, and the use of a simple one-dimensional velocity-density model. We note that the standard deviation from broadband simulations is close to the GMPE standard deviations.

Future work will consider heterogeneous dynamic rupture models with "patchier" slip distributions and more variable rupture propagation. This ensures more efficient seismic radiation of intermediate (1.0 – 3 Hz) and higher frequencies (above 3 Hz). The intermediate range has to be emitted by the rupture to ensure proper radiation characteristics and the transition from double-like radiation to

isotropic radiation in the frequency range 1-4 Hz (Pulido and Kudo, 2004; Spudich and Chiou, 2008). The high-frequency scattering is inherently isotropic, and does not represent the radiation-pattern properties in the frequency range 1.0 – 3 Hz. In conclusion, hybrid broadband ground-motion simulation using spontaneous dynamic ruptures have the potential to provide realistic time series for earthquake-engineering and seismic hazard purposes.

## REFERENCES

- Anderson, J.G., and S.E. Hough (1984). A model for the shape of the Fourier amplitude spectrum of acceleration at high frequencies, *Bull. Seism. Soc. Am.*, 74, 1969-1993.
- Atkinson, G. M., and W. Silva (1997). An empirical study of earthquake source spectra for California earthquakes, *Bull. Seismol. Soc. Am.* 87, 97-113
- Boore DM (1983) Stochastic simulation of high frequency ground motions based on seismological models of the radiation spectra. *Bull Seismol Soc Am*73:1865-1894
- Borcherdt RD (1994) Estimates of site-dependent response spectra for design (methodology and justification). *Earthquake Spectra* 10(4):617-653
- Borcherdt RD (2002) Empirical evidence for acceleration-dependent amplification factors. *Bull Seis Soc Am.* 92(2):761-782
- Dalguer, L.A. and M. Mai (2008), Implications of Style-of-Faulting and Loading Characteristics on the Dynamic Rupture Process, *Eos Trans. AGU*, 89(53), Fall Meet. Suppl., Abstract S51D-1798
- Edwards, B, D. Faeh, B. Allmann, and V. Poggi (2009). Stochastic ground-motion model for Switzerland, *Internal report submitted to the Pegasos Refinement Project Nov. 30, 2009.*
- Graves, R.W. and A. Pitarka (2010), Broadband Ground-Motion Simulation Using a Hybrid Approach, *Bull. Seis. Soc. Am.*, Vol. 100, No. 5A, pp. 2095-2123, October 2010, doi: 10.1785/0120100057
- Guatteri, M., P.M. Mai, G.C. Beroza, and J. Boatwright (2003). Strong-ground motion prediction from stochastic-dynamic source models, *Bull. Seis. Soc. Am.*, Vol. 93 (1), pp. 301-313.
- Hough, S.E., and J.G. Anderson (1988). High-frequency spectra observed at Anza, California – Implications for Q-structure, *Bull. Seis. Soc. Am.*, Vol 78, 692-707
- Mai, P.M., G.C. Beroza (2000). Source-scaling properties from finite-fault rupture models, *Bull. Seis. Soc. Am.*, Vol. 90, pp. 604-615.
- Mai, P.M., and G.C. Beroza (2002). A spatial random-field model to characterize complexity in earthquake slip, *J. Geophys. Res.*, Vol. 107 (B11), 2308, doi:10.1029/2001JB000588.
- Mai, P.M., and G.C. Beroza (2003). A hybrid method for calculating near-source broadband seismograms: application to strong motion prediction, *Phys. Earth Planet. Int.*, 137, 183-199
- Mai, P.M. (2009) Ground Motion: Complexity and Scaling in the Near Field of Earthquake Ruptures, in *Encyclopedia of Complexity & Systems Science*, W.H.K. Lee and R. Meyers (Eds.), Springer, pp 4435-4474.
- Mai, P.M., W. Imperatori, and K.B. Olsen (2010). Hybrid Broadband Ground-Motion Simulations: Combining Long-Period Deterministic Synthetics with High-Frequency Multiple S-to-S Backscattering *Bull. Seis. Soc. Am.*, Vol. 100, No. 5A, pp. 2124-2142, doi: 10.1785/0120080194
- Mena, B., P.M. Mai, K.B. Olsen, M. Purvance, and J. Brune (2010). Hybrid Broadband Ground-Motion Simulation Using Scattering Green's Functions: Application to Large-Magnitude Events, *Bull. Seis. Soc. Am.*, Vol. 100, No. 5A, pp. 2143-2162, doi: 10.1785/0120080318
- Mena, B., and P.M. Mai (2011), Selection and quantification of near-fault velocity pulses owing to source directivity. *Georisk*, Volume 5, Issue 1, March 2011, pages 25-43.
- Pitarka A, Somerville P, Fukushima Y, Uetake T, Irikura K (2000) Simulation of near-fault strong-ground motion using hybrid Green's function. *Bull Seis Soc Am*90(3):566-586
- Pulido, N., and T. Kubo (2004), Near-fault strong motion complexity of the 2000 Tottori earthquake (Japan) from a broadband source asperity model, *Tectonophys.*, 390 (1-4), 177-192.
- Ripperger, J., P. M. Mai and J.-P. Ampuero (2008) Variability of near-field ground motion from dynamic earthquake rupture simulations *Bull. Seism. Soc. Am.*, 98 (3), 1207-1228; doi:10.1785/0120070076
- Shakal AF, Haddadi HR, Huang MJ (2006) Note on the Very-High-Acceleration Fault Zone 16 Record from the 2004 Parkfield Earthquake. *Bull. Seis. Soc. Am.* 96(3):S119-S128
- Spudich, P., and B. S. J. Chiou (2008), Directivity in NGA earthquake ground motions: Analysis using isochrone theory, *Earthquake Spectra*, 24 (1), 279-298, doi:10.1193/1.2928225
- Zeng YH, Su F, Aki K (1991) Scattering wave energy propagation in a random Isotropic scattering medium. 1. Theory *J Geophys Res* 96(B1): 607-619.
- Zeng YH (1993) Theory of scattered P-wave and S-wave energy in a random isotropic scattering medium. *Bull Seis Soc Am* 83(4):1264-12.